Geophysical Research Letters

RESEARCH LETTER
10.1029/2023GL105342

# Tidally Modulated Glacial Slip and Tremor at Helheim Glacier, Greenland

**Peng Yan[1], David M. Holland[1], Victor C. Tsai[2], Irena Vaňková[3], and Surui Xie[4]**

[1]Courant Institute of Mathematical Sciences, New York University, New York, NY, USA, [2]Department of Earth, Environmental and Planetary Sciences, Brown University, Providence, RI, USA, [3]Los Alamos National Laboratory, Los Alamos, NM, USA, [4]Department of Civil and Environmental Engineering, University of Houston, Houston, TX, USA

**Key Points:**

- Multi-year seismic records reveal glacial slip and tremor variability at Helheim Glacier
- Tremor correlates with high effective pressure at tidal timescales, opposite to the expectation at longer timescales
- The tremor source points to an upstream subglacial ridge

**Supporting Information:**

Supporting Information may be found in the online version of this article.

**Correspondence to:**

P. Yan,
py15@nyu.edu

**Citation:**

Yan, P., Holland, D. M., Tsai, V. C., Vaňková, I., & Xie, S. (2024). Tidally modulated glacial slip and tremor at Helheim Glacier, Greenland. *Geophysical Research Letters*, *51*, e2023GL105342. https://doi.org/10.1029/2023GL105342

Received 22 JUL 2023
Accepted 30 NOV 2023

**Abstract** Numerical modeling of ice sheet motion and hence projections of global sea level rise require information about the evolving subglacial environment, which unfortunately remains largely unknown due to its difficulty of access. Here we advance such subglacial observations by reporting multi-year observations of seismic tremor likely associated with glacier sliding at Helheim Glacier. This association is confirmed by correlation analysis between tremor power and multiple environmental forcings on different timescales. Variations of the observed tremor power indicate that different factors affect glacial sliding on different timescales. Effective pressure may control glacial sliding on long (seasonal/annual) timescales, while tidal forcing modulates the sliding rate and tremor power on short (hourly/daily) timescales. Polarization results suggest that the tremor source comes from an upstream subglacial ridge. This observation provides insights on how different factors should be included in ice sheet modeling and how their timescales of variability play an essential role.

**Plain Language Summary** The Greenland Ice Sheet has lost ice increasingly in the past few decades, contributing significantly to global sea level rise. However, large uncertainties remain in computer simulations of such ice mass loss and hence sea level rise. This uncertainly is mainly attributed to the lack of information on what is happening at the bottom of the ice sheet and how that affects ice sheet movement. For example, how much water is there and whether it is in isolated pockets or is well distributed as a thin sheet can have an important effect on ice movement. In this paper, we observe small ground motions that are generated during glacier movement at a marine-terminating glacier in Greenland. By analyzing the energy variation of the small ground motions over multiple years as well as observing the reasons that cause the variations, we learn that subglacial water pressure may control ice flow speeds on a seasonal/annual scale, and that ocean tides can change ice flow on an hourly/daily scale. This observation provides important constraints for computer simulations of future sea level rise in terms of the impacting factors and their respective timescales.

## 1. Introduction

Greenland outlet glaciers draining mass into the ocean through subglacial melting and iceberg calving account for about half of the total ice loss of the Greenland Ice Sheet (Choi et al., 2021; Howat et al., 2007; Mankoff, Solgaard, et al., 2020; Van den Broeke et al., 2016). The subglacial environment (i.e., subglacial hydraulic system and the ice-bed interface coupling state) of outlet glaciers serves as an important boundary condition in glacier models used in projections of global sea level but remains largely unknown due to its difficulty of access, especially for fast-flowing tidewater glaciers (Aschwanden et al., 2016; Bougamont et al., 2014; Clarke, 2005; Goelzer et al., 2017). With in situ observations through boreholes, knowledge regarding glacier sliding has been improved over the past half-century. In particular, the theory of glacial sliding has advanced from the Weertman–style viscous flow and regelation (Weertman, 1957) to the inclusion of cavitation processes at the lee side of protruding clasts (Lliboutry, 1968; Schoof, 2005), and from idealized hard-bedded (non-deformable) sliding to the more realistic soft-bedded deformation and spatially heterogeneous sliding scenarios (Alley et al., 2023; Clarke, 2005; Tsai et al., 2015, 2022; Zoet & Iverson, 2020). Rheological experiments have also helped improve our understanding of glacier sliding (Iverson et al., 1998; Leeman et al., 2016; Nye, 1953; Tulaczyk et al., 2000). Though borehole drilling provides important direct information about the subglacial environment, the high cost and labor-intensive requirements limit its application, especially for fast-flowing tidewater glaciers. The nature of moving ice often inhibits repeated drilling at the same location to retrieve information on the evolving subglacial environment over long and continuous periods. Thus, there is a pressing need to seek appropriate observational

approaches to decipher and monitor subglacial processes occurring at the ice-bed interface to improve the accuracy of the ice sheet components of climate models (Catania et al., 2020; Goelzer et al., 2017).

Passive seismology has been increasingly harnessed by the glaciology community due to its cost- and labor-effectiveness and the ability to remotely sense processes within and beneath ice continuously (Aster & Winberry, 2017; Podolskiy & Walter, 2016). To date, discrete basal icequakes that reveal mechanisms of ice movement over the bed have been reported at Antarctic ice streams, the Greenland Ice Sheet, and alpine glaciers (e.g., Anandakrishnan & Alley, 1997; Barcheck et al., 2018; Danesi et al., 2007; Gräff et al., 2021; Helmstetter et al., 2015; Hudson et al., 2020; Kufner et al., 2021; McBrearty et al., 2020; Roeoesli et al., 2016; VanWormer & Berg, 1973; Weaver & Malone, 1979; Winberry et al., 2013; Zoet et al., 2012). The magnitudes of the reported basal seismic events range from ∼7 at Whillans Ice Stream to negatives in most other ice environments, which suggest different subglacial conditions and different source patch sizes. Tremor signals (i.e., small and sustained seismic events) associated with stick-slip observed during short summer campaigns have also been reported in some ice environments (Lipovsky & Dunham, 2016; Umlauft et al., 2021; Winberry et al., 2013). Recently, an ocean-bottom seismometer, together with surface seismometers, was used for the first time to reveal glacial sliding by recording seismic tremors at an outlet glacier in Greenland (Podolskiy et al., 2021).

A number of environmental forcings have been reported to impact glacier sliding at Helheim Glacier, a large fast-flowing glacier in East Greenland that has been losing ice rapidly over the past few decades (Andresen et al., 2012; Howat et al., 2005; Khan et al., 2020; Nick et al., 2009; Straneo et al., 2011). These include instantaneous speedup caused by iceberg calving (Nettles et al., 2008), short-term (multi-days, daily or sub-daily) speed variations due to meltwater production and tidal forcing (De Juan et al., 2010; Stevens et al., 2022; Voytenko et al., 2015), and long-term speed variations in response to evolving terminus conditions (Ultee et al., 2022). In this study, we for the first time report multi-year continuous observations of tremor signals that are likely associated with subglacial sliding at Helheim Glacier, together with a suite of supporting data that recorded different environmental forcings in a summer campaign. We will discuss how the tremor signal is attributed to glacier sliding and how competing hypotheses can be ruled out by correlation analysis when considering multiple environmental forcings. We will also illustrate the possible tremor locations using a single station-based polarization method. This observation provides important insight into advancing modeling of ice mass balance on different timescales, in which information on the basal environment and its evolution are important parameters that need to be taken into account (Goelzer et al., 2017; Tsai et al., 2022).

## 2. Data and Methods

### 2.1. Study Site

Helheim is one of the highest-flux outlet glaciers in Greenland and has drawn significant attention from the scientific community in the past few decades (Nettles et al., 2008; Stearns & Hamilton, 2007), including for the project in which we organized an intensive suite of instrumentation to investigate glacier dynamics at Helheim (Holland et al., 2016). Specifically, four broadband seismometers (site HEL1 had a Nanometrics Trillium 120 device, and sites HEL2, HEL3, and HEL4 had Nanometrics Trillium 240 devices) were deployed on bedrock outcrops around the glacier terminus since 2012, with two stations on each side within a distance of 3 km to the glacier centerline (Figure 1). Co-located with HEL1 is an automated weather station (AWS). At the HEL2 site, a high spatiotemporal resolution terrestrial radar interferometer (TRI) that can be used to infer ice motion and volume changes was deployed between August 6 and 12, 2016. An array of autonomous phase-sensitive radio-echo sounders (ApRES) that are capable of detecting internal reflectors due to changes in electromagnetic properties within ice was also deployed along a central flowline in August of 2016 (Vaňková et al., 2018).

### 2.2. Seismic Processing

We calculate median power spectral densities (PSD) using the vertical component of seismic records collected between deployment date and August of 2017 for each station (except for data gap periods caused by datalogger storage issues, Figure S1 in Supporting Information S1). Following Bartholomaus et al. (2015), we use 20 s short-duration and 30 min long-duration windows to calculate and refine the individual PSDs, respectively, with 50% overlapping time windows. Preceding the PSD calculations, we apply basic preprocessing such as instrument response removal (to obtain velocity seismograms). We then calculate integrated tremor power over

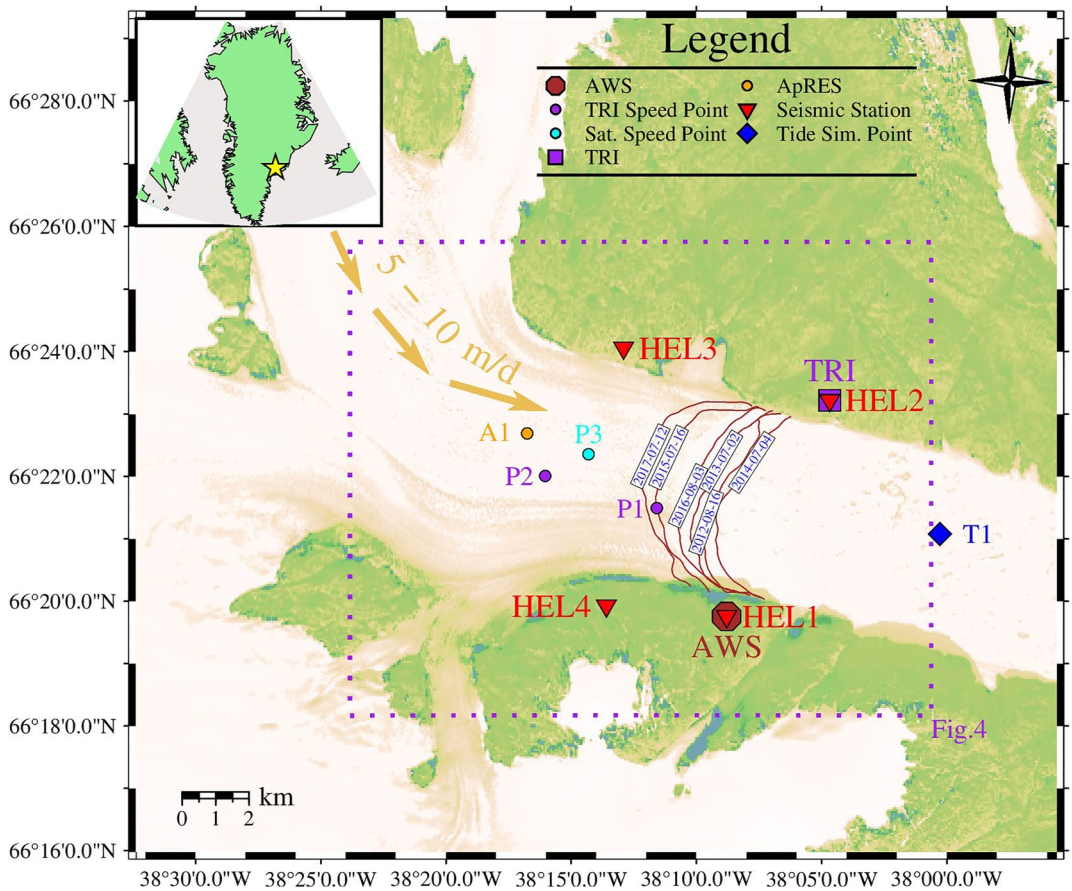


**Figure 1.** Details of the study site. Multi-source observational instrumentation at Helheim Glacier (background satellite image from Lansat-8 acquired on 17 August 2016), including continuous observations of four bedrock-deployed broadband seismometers (i.e., HEL1, HEL2, HEL3, HEL4), an autonomous-phase sensitive radio echo sounder (ApRES), and an automatic weather station (AWS). ApRES (A1) operated during August 2016. A terrestrial radar interferometer (TRI) was deployed from 6 to 12 August 2016. P1 and P2 are two points where Line- of-Sight (LOS) ice flow speed is determined from TRI. P3 is where mean surface speed is derived from satellite observations. T1 is where tide height was calculated, ~7 km away from the delineated calving front on 3 August 2016. Lightbrown arrows show the ice flow direction. Arched red lines spanning the ice front indicate the terminus positions on various dates (Cheng et al., 2021). Dashed line box outlines area shown in Figure 4.

different frequency bands (2–10 Hz, 10–20 Hz, and 20–80 Hz) during the observational periods for each station. Though we consider different frequency bands for the PSD calculations, we adopt the 2–10 Hz band to display tremor power results in this study since the tremor power in the three frequency bands exhibit similar variations and the 2–10 Hz band has the largest power levels (Figure S2 in Supporting Information S1).

We determine tremor source locations from a frequency-dependent polarization analysis (FDPA), which can be used to measure azimuths and phase types from a three-component seismogram at given frequencies (Park et al., 1987). To apply the FDPA method, we window the continuous seismic data for each station into 7 min segments and transform the data into the frequency domain via the Fast Fourier Transform (FFT) to form the averaged spectral covariance matrices over the 2–10 Hz band. After that, we perform a singular value decomposition (SVD) on the matrices to find the largest eigenvalue and the corresponding eigenvector, which is associated with the polarization vector (phase). Detailed FDPA processing procedures are described by Vore et al. (2019) and Clyne et al. (2023). Back azimuth can be determined directly from the FDPA when the waveform is Rayleigh (P-SV)-wave polarized and the propagation directions can also be estimated when the dominant polarization type is a body wave, both of which illustrate the tremor source directions. While Love (P-SH) waves also exhibit linear motion, our data set shows equal or slightly less power in the vertical direction than in the horizontal directions, which indicates P or SV waves rather than SH waves occur. Given that we are not interested in the particular

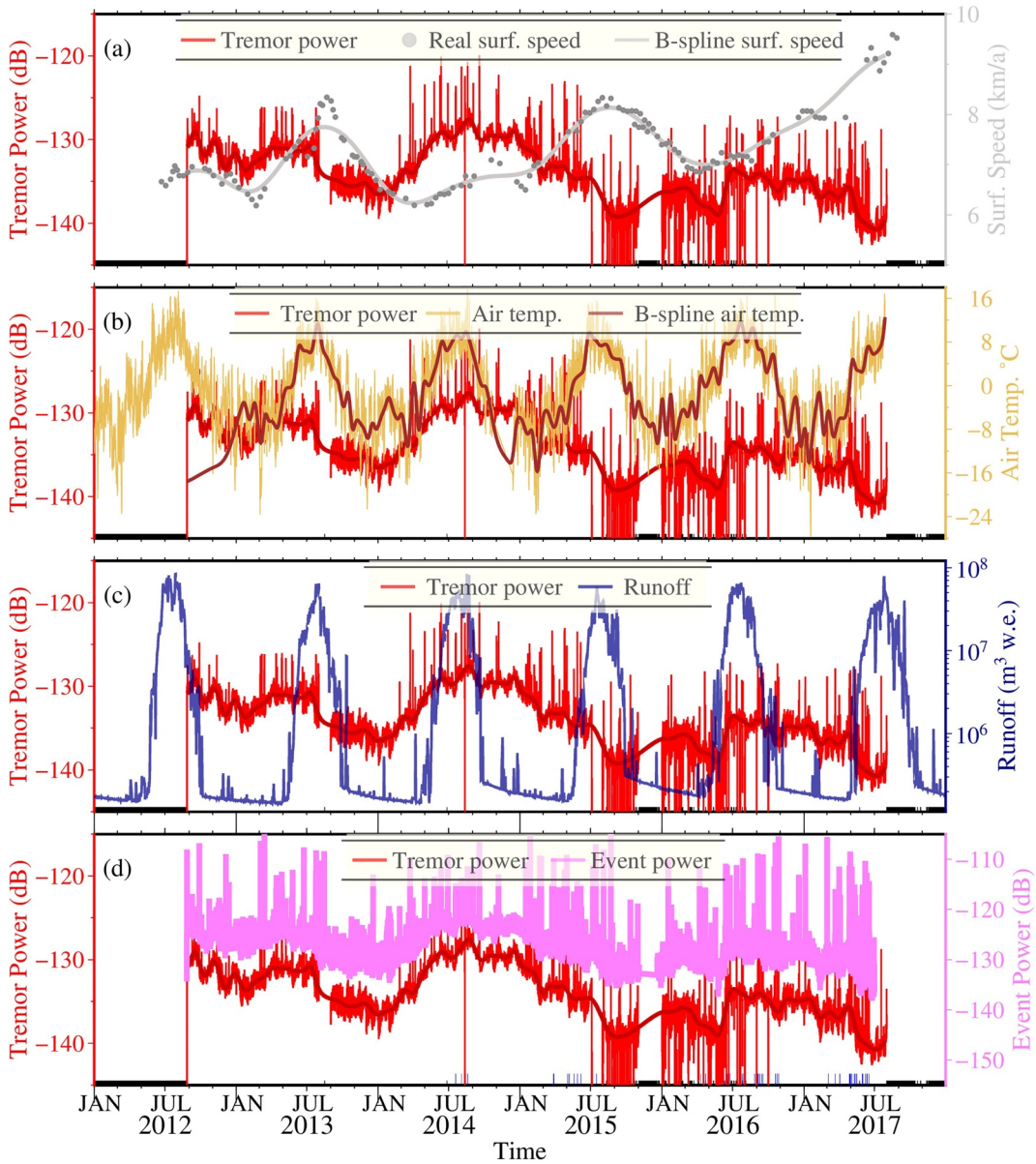


**Figure 2.** Annual variations of integrated tremor power (2–10 Hz) and environmental forcings from August 2012 to June 2017 for station HEL1. Tremor power (in units of dB relative to $(m/s)^2/Hz$) is shown in red in panels (a–d). Black bars at the bottom of each panel indicate data gaps in seismic records. (a) 125 discrete measurements (dots) and B-spline interpolated continuous surface speed (line) at the P3 point (Figure 1). (b) Continuous air temperature record at HEL1 (Figure 1). (c) Catchment-integrated runoff from RACMO2 (Noël et al., 2018). (d) Summed moving-averaged power of discrete seismicity (detected in the same 2–10 Hz band as the tremor signal). Similar plots for stations HEL2, HEL3, and HEL4 are shown in Figure S8 in Supporting Information S1.

polarization wave types as in hydraulic tremor studies (Clyne et al., 2023; Vore et al., 2019), we do not make a clear distinction between back azimuth and propagation direction estimated from Rayleigh-wave and body-wave polarizations, respectively, but refer to them as tremor source direction uniformly hereafter.

### 2.3. Environmental Forcings

We estimate long-term (i.e., seasonal and annual) ice surface velocity from interpolating 125 discrete satellite observations from August 2012 to August 2017 using the B-spline approach (Riel et al., 2021). One location (P3) along a central flowline is used to show the velocity variation during this period (Figures 1 and 2a; Figure S3 in

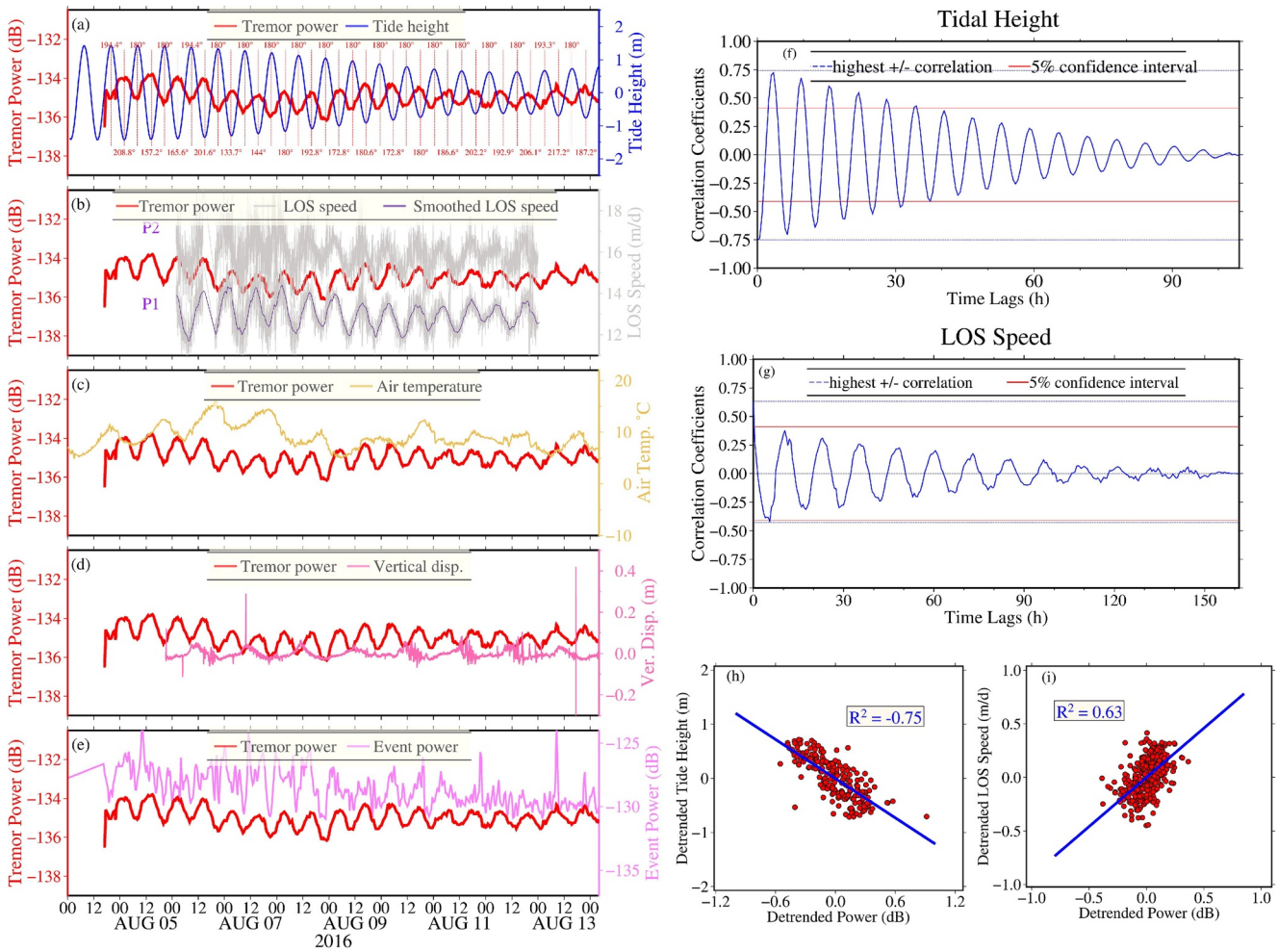


**Figure 3.** Daily variations of integrated tremor power (2–10 Hz) and environmental forcings from 4 to 13 August 2016 for station HEL1. Tremor power is shown in red in panels (a–e). (a) Tidal heights are simulated at T1 (Figure 1) using the TMD package (Erofeeva et al., 2020). Phase shifts between tremor power and tidal height at each peak and trough (vertical dashed lines) are shown in this panel. (b) TRI determined LOS surface ice flow speeds at P1 and P2 (Figure 1). Note the speed at P2 is larger than that at P1 because they are shown in the radar polar coordinate system. (c) Air temperature. (d) Daily variations of ApRES depth-cumulative displacements above 300 m depth at A1 (Figure 1). (e) Summed and moving-average power of discrete seismicity. Similar plots for station HEL4 are shown in Figure S10 in Supporting Information S1. (f) Cross-correlation between tremor power and tidal height. (g) Cross-correlation between tremor power and smoothed LOS speed at P1 (thin purple line in panel (b)). (h) Scatter plot showing the correlation between tremor power and tidal height ($R^2$ the Pearson correlation coefficient). (i) Scatter plot showing the correlation between tremor power and LOS speed at P1.

Supporting Information S1). Short-term (i.e., hourly/daily) Line-of-Sight (LOS) ice flow speed is obtained from the terrestrial radar interferometer after being processed with procedures described in Voytenko et al. (2015), Xie et al. (2019), and Wang et al. (2022). LOS velocity variations at two locations (P1 and P2, Figure S4 in Supporting Information S1) are shown in Figure 3b. Hourly horizontal strain rates are also calculated using the TRI data set (Figure S5 in Supporting Information S1).

Daily runoff during 2012 and 2017 is derived from the regional climate model RACMO2 (Noël et al., 2018) over the Helheim Glacier catchment defined by Mankoff, Noël, et al. (2020). Short-term (hourly/daily) vertical motion for the internal reflectors at different depths at site A1 (Figure 1) are extracted from ApRES observations during August 2016 (sampled at 1-min intervals). Specifically, displacement time series of depth-cumulative motion of internal reflectors at 300 m depth are used in this study. Data processing details and depth-cumulative displacements at other depths (e.g., 100 and 900 m) that all change in phase can be found in Vaňková et al. (2018).

Air temperature between 2012 and 2017 is derived from the AWS deployed at the HEL1 site. The 10 min-sampled air temperature is later smoothed to have the same sampling rate as tremor power for cross-correlation analysis.

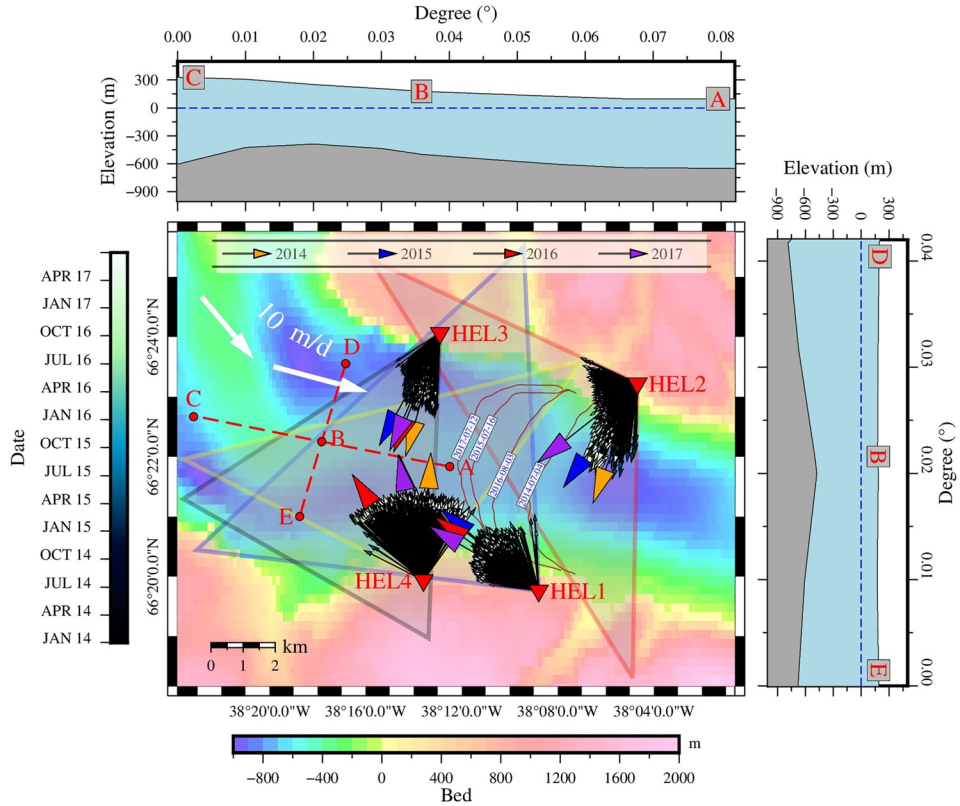


**Figure 4.** Tremor source direction estimates determined from FDPA. Small arrows represent daily averaged source direction angles of different dates, and arrow lengths denote confidence levels of the determined source direction results, normalized among the four stations. Large orange, blue, red, and purple arrows represent weighted average source directions (Table S1 in Supporting Information S1) for 2014, 2015, 2016, and 2017, respectively (Figure S11 in Supporting Information S1). Possible tremor source locations are constrained within the area determined by the maximum and the minimum direction angles of each station. Note that the triangular areas do not represent exact source regions but rather the range of possible source directions, and could extend farther than shown. An overlap area that covers a subglacial ridge by the network can be found. Two profiles (lines ABC and DBE) show elevation variations near the ridge. White thick arrows denote flow direction. Underlying shaded colors represent bedrock elevation (Morlighem et al., 2017).

Tidal height (including M2 and S2 constituents) is simulated at the T1 point in the fjord, ~7 km away from the calving front (delineated on 3 August, 2016) using the Greenland 1 km Tide Model (Howard & Padman, 2021) with the Tide Model Driver (TMD) toolbox (Erofeeva et al., 2020).

## 3. Results

Tremor power at the four stations all exhibit somewhat similar long-term trends from 2012 to 2017 during overlapping observation periods (Figure S6 in Supporting Information S1). Since all stations have similar power variations and HEL1 has the most complete seismic records, we use HEL1 to illustrate the power variation from 2012 to 2017 and its correlation relationships with environmental forcings in this study.

As shown in Figure 2; Figure S6 in Supporting Information S1, no consistent annual/seasonal variations of tremor power are observed from 2012 to 2017. Specifically, tremor power appears to increase in January 2013 and 2014 but not so clearly in other years, and reaches a local maximum in July or August in 2013 and 2014, but appear to have opposite trends in 2015 and 2017. Tremor power also changes abruptly sometimes, as in June and July 2016. The aforementioned features of long-term (i.e., monthly/annually) tremor power variations fail to have a clear positive/negative correlation relationship with surface ice speed (Figure S7a in Supporting Information S1). In some periods, changes in tremor power correlate positively with changes in surface ice speed (i.e., August 2012–July 2013 and January–July 2014), but sometimes not (i.e., March 2015–May 2016 and May–July 2017, Figure 2a). Long-term tremor power variations also do not show a clear correlation with other

environmental forcings such as air temperature (Figure 2b; Figure S7b in Supporting Information S1) and daily runoff (Figure 2c), which both exhibit clear and consistent seasonal fluctuations (i.e., peaks in summer seasons and troughs in winter seasons). Similar results for HEL2, HEL3, and HEL4 stations can be found in Figure S8 in Supporting Information S1. As will be elaborated more in the Discussion, tremor power does correlate well with the summed power of individual seismic events detected in the same 2–10 Hz band (Text S1 in Supporting Information S1 and Figure 2d; Figure S9 in Supporting Information S1).

While long-term environmental forcing does not explain most tremor variability, tremor power exhibits a clear and consistent semidiurnal period on short timescales (i.e., hourly/daily, Figure 3). This clear semidiurnal variability motivates us to investigate the correlation relationships between tremor power and environmental forcings on such timescales. As shown in Figure 3a, there is a strong negative correlation between tremor power and tidal height. Tremor peaks are always observed during low tide periods, while tremor troughs consistently appear during periods of high tide, with a correlation coefficient between tremor and tidal height of −0.75 (Figures 3f and 3h). This is consistent across all seasons during the observation period (Figure S10 in Supporting Information S1). In addition, a positive correlation between tremor power and LOS ice speed (derived from TRI measurements in August 2016) can be found over the short time period of TRI observations (Figure 3b) with a correlation coefficient of 0.63 (Figures 3g and 3i). No clear correlations, however, can be found between tremor power and air temperature and vertical displacements of glacier internal reflectors, which instead both show diurnal variations (Figures 3c and 3d) rather than semidiurnal variations.

Daily averaged tremor source directions determined from the network between June 2014 and June 2017 (the overlapping working period) using FDPA are shown in Figure 4; Figure S11 in Supporting Information S1. There are 1025, 603, 641, and 691 daily source direction estimates for HEL1, HEL2, HEL3, and HEL4, respectively. Despite HEL1 having the largest number of daily source direction estimates, the deviation of the estimated daily source directions from the average is the smallest amongst the four stations (Figure 4). In contrast, HEL2 has less consistent direction estimates compared to the other three stations. Weighted average source directions for each station in each single year are calculated (Table S1 in Supporting Information S1) and shown as large colored arrows in Figure 4; Figure S11 in Supporting Information S1. The weighted average source directions vary within 15° at HEL1 and HEL3 in different years, and changes no more than 35° at HEL2 and HEL4. We note that HEL1 and HEL3's and a certain portion of HEL2 and HEL4's daily direction estimates are consistent with the location of a subglacial ridge in the common coverage area (Morlighem et al., 2017). This subglacial ridge may be the source location for the tremor and will be discussed next.

## 4. Discussion

In previous studies, 2–10 Hz tremor has been interpreted to be caused by water discharge (Bartholomaus et al., 2015; Clyne et al., 2023; Eibl et al., 2020; Lindner et al., 2020; Vore et al., 2019). In those studies, tremor amplitude is correlated well with subglacial water discharge, and tremor amplitude is also found to be in phase with surface melt (the primary source of subglacial discharge). However, tremor at Helheim is neither correlated with discharge nor temperature (and thus melt). Tremor power shows no correlation with runoff on long timescales (Figure 2c) and there is also no correlation with diurnal surface melt-driven vertical displacements of internal reflectors derived from ApRES measurement on short timescales (Figure 3d).

Surface crevassing has also been widely reported in different glacier environments (Aster & Winberry, 2017; Podolskiy & Walter, 2016) and a possible cause of tremor. However, tremor at Helheim is probably not dominantly caused by surface crevassing. First of all, the likely tremor source locations determined from the network point to a region 5 km upstream from the terminus (the mean position between 2012 and 2017), rather than the most crevassed calving front (Figure 4). Although some surface crevasses and supraglacial ponds can also be found in the upstream region (Everett et al., 2016), the meltwater- and/or temperature -driven crevassing opening and closing process will result in a diurnal rather than a semi-diurnal variation of tremor power as is observed here (Figures 3c and 3d). Since surface crevassing due to tidally driven ice stretching (mostly during falling tide) has been reported at Bowdoin Glacier to also cause tremor (Podolskiy et al., 2016, 2021), we investigated whether strain rates (Figure S5 in Supporting Information S1) might explain the tremor power variability. There is no clear correlation between tremor power and strain rates (Table S2 in Supporting Information S1), with the strain rate variability not having a clear tidal modulation (Figure S12 in Supporting Information S1). Instead, 17 out of 36 tremor peaks (troughs) appear at exactly low (high) tide (i.e., 180° phase shift, to the phase resolution of the

measurements), and the phase shifts for the rest of the peaks (troughs) range between 133.7° and 217.2° (note the phase resolution is ∼15° for both tremor power and tidal height time series). Thus, the observed tremor is not related to the main observed strain rate variability and also does not occur with the falling tide, and is therefore inconsistent with the model for crevassing from tidally driven ice stretching. Although we find surface crevassing to be an unlikely source of the tremor signal for the reasons above, surface crevassing and its significant complicating effects on seismic wave propagation cause significant uncertainties in tremor source direction estimates. This uncertainty is highest at HEL2 where ice fracturing frequently occurs near the calving front and in the mélange.

It has been demonstrated that high tide resists and slows ice flow, while low tide promotes sliding at Helheim using ∼50 hr of TRI data set collected in 2013 (Voytenko et al., 2015). This is consistent with the correlation relationship between tidal height and LOS speed derived from the TRI data set collected in 2016, that is, a negative correlation coefficient (−0.66) with a 1.5-hr phase lag (Figure S13 in Supporting Information S1). Meanwhile, our observations show that tremor power is both well correlated with tidal height (negatively, consistently in both summer and winter; Figure S10 in Supporting Information S1) and LOS ice speed (positively) on short timescales (Figure 3b). The tidally modulated glacial slip observed at Helheim and the good correlation between tremor power and tides and LOS ice speed and the poor correlation with other environmental forcings (i.e., strain rates, air temperature, runoff, and internal glacier hydraulic processes (revealed by ApRES)) suggests that the tremor is associated with glacial sliding. The contact stress tidal modulation model of Robel et al. (2017) may serve as a first-order explanation, with increased contact stresses at low tide and thus increased average basal friction. Similar tremor signals associated with glacier sliding have also recently been reported at Bowdoin Glacier, which was recorded by an ocean bottom seismometer and surface seismometers. The tremor signal observed there was also found to be correlated well with GPS measurements and modulated by the tide in several short field campaigns (Podolskiy et al., 2021).

The overlapping area determined by the tremor source directions estimated from the network using FDPA indicates the tremor source may come from the region associated with the subglacial ridge ("the ridge" hereafter, Figure 4), consistent with the Robel et al. (2017) model in which tidally modulated pinning point migration can influence flow variations. This location would explain why power levels at HEL3 and HEL4 are generally higher than that at HEL1 and HEL2 (less geometric attenuation for the shorter distances, Figure S6 in Supporting Information S1). The ridge zone may be responsible for tremor because the shallower subglacial bed increases the effective friction. We cannot determine whether the tremor/seismicity occur at the ice-bed interface and/or within subglacial ice, which is commonly acknowledged to be a challenging issue (Köpfli et al., 2022; Walter et al., 2008). Nonetheless, we infer that the tremor observed here probably occurs at the ice-till layer or within the till layer within the ridge zone since a lot of debris-laden icebergs calved from the glacier terminus are observed (Holland et al., 2016) and inferred from sediment core records (Andresen et al., 2012). Such tremor/seismicity can occur in the form of particle failure/friction when ice slides over protruding rocks or the moving ice plows through the till layer. This suggestion could potentially be verified with high-resolution subglacial topography derived from surface and/or airborne penetrating radar (Bingham et al., 2017). Additionally, inclusion of on-ice or borehole sensors deployed within the region would be useful to further refine the source locations and to determine source mechanisms (Gräff et al., 2021).

Given our best interpretation of tremor as a subglacial source, observed temporal variations in tremor power provide important insights into the evolving subglacial environment and its impact on different timescales. Several reasons may account for the observed tremor power variations at HEL1. First, ice thickness (weight) that accumulates or shrinks on long timescales (annually/seasonally) controls the gravitational driving force that drives ice flow (Cuffey & Paterson, 2010), though this is unlikely significant over the relatively short observation period. Second, changes in water pressure that impact effective pressure (ice overburden pressure minus the water pressure) around the source patch(s) at the ice-bed interface can greatly modulate sliding speeds and till deformation rates (Gräff & Walter, 2021; Hart et al., 2019; Lipovsky et al., 2019; Tsai et al., 2022). A lower effective pressure (generally during early summer seasons) facilitates sliding at the ice-bed interface, resulting in higher tremor power levels, and vice versa for the winter seasons. The transition of tremor power from summer to winter is not expected to occur abruptly but gradually as observed here. Short (hours) and long (days) cycles of subglacial sliding and deformation during summer and winter, respectively, have been observed at an Icelandic tidewater glacier using subglacial till probes (Hart et al., 2019); the long time for accommodating meltwater in winter may explain why the tremor power at Helheim does not decrease abruptly at the beginning of winter but instead remains at a low power level throughout the winter (Figure 2). Abrupt calving events or outbursts of

meltwater that change water pressure and the force balance suddenly and episodically may be responsible for the few times of abrupt changes of tremor powers observed at Helheim, though independent confirmation of this is lacking. Changes in water pressure are also expected due to the evolution of subglacial drainage systems (cavities and channels) on a seasonal timescale and may explain some of the observed variability. Finally, on short timescales, effective pressure and friction are modulated by the tide as is observed here. Specifically, effective pressure reaches a maximum at low tide and a minimum during high tide. The observed tremor peaks during low tide are consistent with this since subglacial slip speeds increase at low tide (with the Robel et al. (2017) "Bindschadler" style model attributing this to increased hydrostatic driving stress), which in turn results in higher frictional stressing rate and hence higher tremor rates due to the enhanced basal contact during low tide. Interestingly, this positive correlation between tremor and high effective pressure (low tide) at tidal periods is the opposite sign of correlation to the traditional expectation of increased tremor with enhanced sliding caused by low effective pressure (Schoof, 2010). The current observations therefore indicate that different physics may be important at short tidal timescales compared with at longer timescales and that these complexities in which factors are important may need to be considered in ice sheet modeling for predicting future sea level rise.

Lastly, we note that the strong correlation between tremor and seismicity rate is consistent with the interpretation of tremor being the manifestation of basal microseismicity below the event detection threshold, like for tectonic tremors (Frank et al., 2015). A simple estimate (see Text S2 in Supporting Information S1) suggests that the tremor power is consistent with a family of very small and numerous events drawn from a Gutenberg-Richter size distribution with a $b$ value in the range of 1–2 (Figure S14 in Supporting Information S1), a somewhat higher $b$ value than is typical for typical tectonic earthquakes but similar to what is observed for certain earthquake swarms potentially driven by creep (Jenatton et al., 2007; Wiemer & Wyss, 2002).

## 5. Conclusions

In this work, we have shown that seismic tremor is observed at Helheim Glacier and is likely associated with subglacial slip. We infer that effective pressure variations partially control the observed variability in tremor, both at long timescales (i.e., seasonally and annually, where low effective pressure results in higher tremor) and at short tidal timescales (i.e., hourly and daily, where higher effective pressure results in higher tremor) but with opposite signs of correlation. Continuous observations of tremor at fast-flowing tidewater glaciers may provide an effective way to reveal subglacial conditions and their evolution, particularly effective pressure which greatly impacts sliding and deformation rate at the ice-bed interface and hence ultimately projections of global sea level rise. Despite the timescales and magnitudes of slip variations for glaciers being quite different from that in tectonic subduction zone settings where similar slip tremors occur (Obara, 2002; Rogers & Dragert, 2003), beneath-ice observations also hold the potential to provide insight into studies of earthquake cycles.

## Data Availability Statement

The seismic data set is partially open at IRISDMC (Holland, 2012). Raw seismic waveforms of HEL1 station, the TRI and the ApRES products used for this manuscript have been deposited in the Zenodo databases (Yan et al., 2023a, 2023b, 2023c, 2023d). The MEaSUREs velocity data used in this manuscript are publicly available through the National Snow and Ice Data Center (Joughin et al., 2011). Runoff product used in this manuscript is available the Zenodo database (Ultee, 2021). We used open-source Python toolbox for seismic data processing (Beyreuther et al., 2010). We used the med_spec code for the PSDs calculation (Bartholomaus & Terleth, 2023). Figures were created with the Generic Mapping Tools (GMT) software (V6, Wessel et al., 2019).

**Acknowledgments**
We are grateful to the support provided by NSF grant through PLR-2151295 and PLR-1739003. We thank Denise Holland for organizing field logistics in Greenland. This work was supported in part through the NYU IT High Performance Computing resources, services, and staff expertise. We thank Sheng Minhan for suggestions on figure generations. We thank Denis Voytenko and Xianwei Wang for suggestions on TRI data processing. We thank Bryan Riel for the help with the time series analysis tool for B-spline interpolations. We would like to thank the editor and the reviewers for their helpful comments in improving the manuscript.

## References

Alley, R. B., Holschuh, N., Parizek, B., Zoet, L. K., Riverman, K., Muto, A., et al. (2023). GHOSTly flute music: Drumlins, moats and the bed of Thwaites Glacier. *Annals of Glaciology*, *63*(87–89), 1–5. https://doi.org/10.1017/aog.2023.43

Anandakrishnan, S., & Alley, R. B. (1997). Tidal forcing of basal seismicity of ice stream C, West Antarctica, observed far inland. *Journal of Geophysical Research*, *102*(B7), 15183–15196. https://doi.org/10.1029/97jb01073

Andresen, C. S., Straneo, F., Ribergaard, M. H., Bjørk, A. A., Andersen, T. J., Kuijpers, A., et al. (2012). Rapid response of Helheim Glacier in Greenland to climate variability over the past century. *Nature Geoscience*, *5*(1), 37–41. https://doi.org/10.1038/ngeo1349

Aschwanden, A., Fahnestock, M. A., & Truffer, M. (2016). Complex Greenland outlet glacier flow captured. *Nature Communications*, *7*(1), 10524. https://doi.org/10.1038/ncomms10524

Aster, R. C., & Winberry, J. P. (2017). Glacial seismology. *Reports on Progress in Physics*, *80*(12), 126801. https://doi.org/10.1088/1361-6633/aa8473

Barcheck, C. G., Tulaczyk, S., Schwartz, S. Y., Walter, J. I., & Winberry, J. P. (2018). Implications of basal micro-earthquakes and tremor for ice stream mechanics: Stick-slip basal sliding and till erosion. *Earth and Planetary Science Letters*, *486*, 54–60. https://doi.org/10.1016/j.epsl.2017.12.046

Bartholomaus, T., & Terleth, Y. (2023). med_spec: Calculation of median seismic spectrograms, for purposes of quantifying tremor (version 1.0.0) [Software]. Zenodo. https://doi.org/10.5281/zenodo.8102681

Bartholomaus, T. C., Amundson, J. M., Walter, J. I., O'Neel, S., West, M. E., & Larsen, C. F. (2015). Subglacial discharge at tidewater glaciers revealed by seismic tremor. *Geophysical Research Letters*, *42*(15), 6391–6398. https://doi.org/10.1002/2015gl064590

Beyreuther, M., Barsch, R., Krischer, L., Megies, T., Behr, Y., & Wassermann, J. (2010). ObsPy: A Python toolbox for seismology [Software]. Seismological Research Letters, *81*, 30–533. https://doi.org/10.1785/gssrl.81.3.530

Bingham, R. G., Vaughan, D. G., King, E. C., Davies, D., Cornford, S. L., Smith, A. M., et al. (2017). Diverse landscapes beneath Pine Island Glacier influence ice flow. *Nature Communications*, *8*(1), 1618. https://doi.org/10.1038/s41467-017-01597-y

Bougamont, M., Christoffersen, P., Hubbard, A. L., Fitzpatrick, A. A., Doyle, S. H., & Carter, S. P. (2014). Sensitive response of the Greenland Ice Sheet to surface melt drainage over a soft bed. *Nature Communications*, *5*(1), 5052. https://doi.org/10.1038/ncomms6052

Catania, G. A., Stearns, L. A., Moon, T. A., Enderlin, E. M., & Jackson, R. H. (2020). Future evolution of Greenland's marine-terminating outlet glaciers. *Journal of Geophysical Research: Earth Surface*, *125*(2), e2018JF004873. https://doi.org/10.1029/2018jf004873

Cheng, D., Hayes, W., Larour, E., Mohajerani, Y., Wood, M., Velicogna, I., & Rignot, E. (2021). Calving Front Machine (CALFIN): Glacial termini dataset and automated deep learning extraction method for Greenland, 1972–2019. *The Cryosphere*, *15*(3), 1663–1675. https://doi.org/10.5194/tc-15-1663-2021

Choi, Y., Morlighem, M., Rignot, E., & Wood, M. (2021). Ice dynamics will remain a primary driver of Greenland ice sheet mass loss over the next century. *Communications Earth & Environment*, *2*(1), 26. https://doi.org/10.1038/s43247-021-00092-z

Clarke, G. K. (2005). Subglacial processes. *Annual Review of Earth and Planetary Sciences*, *33*(1), 247–276. https://doi.org/10.1146/annurev.earth.33.092203.122621

Clyne, E., Alley, R. B., Vore, M., Gräff, D., Anandakrishnan, S., Walter, F., & Sergeant, A. (2023). Glacial hydraulic tremor on Rhonegletscher, Switzerland. *Journal of Glaciology*, *69*(274), 370–380. https://doi.org/10.1017/jog.2022.69

Cuffey, K. M., & Paterson, W. S. B. (2010). *The physics of glaciers*. Academic Press.

Danesi, S., Bannister, S., & Morelli, A. (2007). Repeating earthquakes from rupture of an asperity under an Antarctic outlet glacier. *Earth and Planetary Science Letters*, *253*(1–2), 151–158. https://doi.org/10.1016/j.epsl.2006.10.023

De Juan, J., Elósegui, P., Nettles, M., Larsen, T. B., Davis, J. L., Hamilton, G. S., et al. (2010). Sudden increase in tidal response linked to calving and acceleration at a large Greenland outlet glacier. *Geophysical Research Letters*, *37*(12), L12501. https://doi.org/10.1029/2010gl043289

Eibl, E. P., Bean, C. J., Einarsson, B., Pàlsson, F., & Vogfjörd, K. S. (2020). Seismic ground vibrations give advanced early-warning of subglacial floods. *Nature Communications*, *11*(1), 2504. https://doi.org/10.1038/s41467-020-15744-5

Erofeeva, S., Padman, L., & Howard, S. L. (2020). Tide model driver (TMD) version 2.5, toolbox for Matlab.

Everett, A., Murray, T., Selmes, N., Rutt, I. C., Luckman, A., James, T. D., et al. (2016). Annual down-glacier drainage of lakes and water-filled crevasses at Helheim Glacier, southeast Greenland. *Journal of Geophysical Research: Earth Surface*, *121*(10), 1819–1833. https://doi.org/10.1002/2016jf003831

Frank, W. B., Shapiro, N. M., Husker, A. L., Kostoglodov, V., Bhat, H. S., & Campillo, M. (2015). Along-fault pore-pressure evolution during a slow-slip event in Guerrero, Mexico. *Earth and Planetary Science Letters*, *413*, 135–143. https://doi.org/10.1016/j.epsl.2014.12.051

Goelzer, H., Robinson, A., Seroussi, H., & Van De Wal, R. S. (2017). Recent progress in Greenland ice sheet modelling. *Current Climate Change Reports*, *3*(4), 291–302. https://doi.org/10.1007/s40641-017-0073-y

Gräff, D., Köpfli, M., Lipovsky, B. P., Selvadurai, P. A., Farinotti, D., & Walter, F. (2021). Fine structure of microseismic glacial stick-slip. *Geophysical Research Letters*, *48*(22), e2021GL096043. https://doi.org/10.1029/2021gl096043

Gräff, D., & Walter, F. (2021). Changing friction at the base of an Alpine glacier. *Scientific Reports*, *11*(1), 1–10. https://doi.org/10.1038/s41598-021-90176-9

Hart, J. K., Martinez, K., Basford, P. J., Clayton, A. I., Robson, B. A., & Young, D. S. (2019). Surface melt driven summer diurnal and winter multi-day stick-slip motion and till sedimentology. *Nature Communications*, *10*(1), 1599. https://doi.org/10.1038/s41467-019-09547-6

Helmstetter, A., Nicolas, B., Comon, P., & Gay, M. (2015). Basal icequakes recorded beneath an Alpine glacier (Glacier d'Argentière, Mont Blanc, France): Evidence for stick-slip motion? *Journal of Geophysical Research: Earth Surface*, *120*(3), 379–401. https://doi.org/10.1002/2014jf003288

Holland, D. M. (2012). Observation of a glacier calving event using a network of GPS and Seismic sensors [Dataset]. International Federation of Digital Seismograph Networks. https://doi.org/10.7914/SN/YF_2012

Holland, D. M., Voytenko, D., Christianson, K., Dixon, T. H., Mei, M. J., Parizek, B. R., et al. (2016). An intensive observation of calving at Helheim Glacier, East Greenland. *Oceanography*, *29*(4), 46–61. https://doi.org/10.5670/oceanog.2016.98

Howard, S. L., & Padman, L. (2021). *Gr1kmTM: Greenland 1 kilometer tide model, 2021*. Arctic Data Center. https://doi.org/10.18739/A2251FM3S

Howat, I. M., Joughin, I., & Scambos, T. A. (2007). Rapid changes in ice discharge from Greenland outlet glaciers. *Science*, *315*(5818), 1559–1561. https://doi.org/10.1126/science.1138478

Howat, I. M., Joughin, I., Tulaczyk, S., & Gogineni, S. (2005). Rapid retreat and acceleration of Helheim Glacier, east Greenland. *Geophysical Research Letters*, *32*(22), L22502. https://doi.org/10.1029/2005gl024737

Hudson, T. S., Brisbourne, A. M., Walter, F., Gräff, D., White, R. S., & Smith, A. M. (2020). Icequake source mechanisms for studying glacial sliding. *Journal of Geophysical Research: Earth Surface*, *125*(11), e2020JF005627. https://doi.org/10.1029/2020jf005627

Iverson, N. R., Hooyer, T. S., & Baker, R. W. (1998). Ring-shear studies of till deformation: Coulomb-plastic behavior and distributed strain in glacier beds. *Journal of Glaciology*, *44*(148), 634–642. https://doi.org/10.1017/s0022143000002136

Jenatton, L., Guiguet, R., Thouvenot, F., & Daix, N. (2007). The 16,000-event 2003–2004 earthquake swarm in Ubaye (French Alps). *Journal of Geophysical Research*, *112*(B11), B11304. https://doi.org/10.1029/2006jb004878

Joughin, I., Howat, I., Smith, B., & Scambos, T. (2011). MEaSUREs Greenland ice velocity: Selected glacier site velocity maps from InSAR, version 1 [Dataset]. NASA National Snow and Ice Data Center Distributed Active Archive Center. https://doi.org/10.5067/MEASURES/CRYOSPHERE/nsidc-0481.001

Khan, S. A., Bjørk, A. A., Bamber, J. L., Morlighem, M., Bevis, M., Kjær, K. H., et al. (2020). Centennial response of Greenland's three largest outlet glaciers. *Nature Communications*, *11*(1), 5718. https://doi.org/10.1038/s41467-020-19580-5

Köpfli, M., Gräff, D., Lipovsky, B. P., Selvadurai, P. A., Farinotti, D., & Walter, F. (2022). Hydraulic conditions for stick-slip tremor beneath an alpine glacier. *Geophysical Research Letters*, *49*(21), e2022GL100286. https://doi.org/10.1029/2022gl100286

Kufner, S. K., Brisbourne, A. M., Smith, A. M., Hudson, T. S., Murray, T., Schlegel, R., et al. (2021). Not all icequakes are created equal: Basal icequakes suggest diverse bed deformation mechanisms at Rutford Ice Stream, West Antarctica. *Journal of Geophysical Research: Earth Surface*, *126*(3), e2020JF006001. https://doi.org/10.1029/2020jf006001

Leeman, J. R., Valdez, R. D., Alley, R. B., Anandakrishnan, S., & Saffer, D. M. (2016). Mechanical and hydrologic properties of Whillans Ice Stream till: Implications for basal strength and stick-slip failure. *Journal of Geophysical Research: Earth Surface*, *121*(7), 1295–1309. https://doi.org/10.1002/2016jf003863

Lindner, F., Walter, F., Laske, G., & Gimbert, F. (2020). Glaciohydraulic seismic tremors on an Alpine glacier. *The Cryosphere*, *14*(1), 287–308. https://doi.org/10.5194/tc-14-287-2020

Lipovsky, B. P., & Dunham, E. M. (2016). Tremor during ice-stream stick slip. *The Cryosphere*, *10*(1), 385–399. https://doi.org/10.5194/tc-10-385-2016

Lipovsky, B. P., Meyer, C. R., Zoet, L. K., McCarthy, C., Hansen, D. D., Rempel, A. W., & Gimbert, F. (2019). Glacier sliding, seismicity and sediment entrainment. *Annals of Glaciology*, *60*(79), 182–192. https://doi.org/10.1017/aog.2019.24

Lliboutry, L. (1968). General theory of subglacial cavitation and sliding of temperate glaciers. *Journal of Glaciology*, *7*(49), 21–58. https://doi.org/10.1017/s0022143000020396

Mankoff, K. D., Noël, B., Fettweis, X., Ahlstrøm, A. P., Colgan, W., Kondo, K., et al. (2020). Greenland liquid water discharge from 1958 through 2019. *Earth System Science Data*, *12*(4), 2811–2841. https://doi.org/10.5194/essd-12-2811-2020

Mankoff, K. D., Solgaard, A., Colgan, W., Ahlstrøm, A. P., Khan, S. A., & Fausto, R. S. (2020). Greenland Ice Sheet solid ice discharge from 1986 through March 2020. *Earth System Science Data*, *12*(2), 1367–1383. https://doi.org/10.5194/essd-12-1367-2020

McBrearty, I. W., Zoet, L. K., & Anandakrishnan, S. (2020). Basal seismicity of the Northeast Greenland ice stream. *Journal of Glaciology*, *66*(257), 430–446. https://doi.org/10.1017/jog.2020.17

Morlighem, M., Williams, C. N., Rignot, E., An, L., Arndt, J. E., Bamber, J. L., et al. (2017). BedMachine v3: Complete bed topography and ocean bathymetry mapping of Greenland from multibeam echo sounding combined with mass conservation. *Geophysical Research Letters*, *44*(21), 11051–11061. https://doi.org/10.1002/2017gl074954

Nettles, M., Larsen, T. B., Elosegui, P., Hamilton, G. S., Stearns, L. A., Ahlstrøm, A. P., et al. (2008). Step-wise changes in glacier flow speed coincide with calving and glacial earthquakes at Helheim Glacier, Greenland. *Geophysical Research Letters*, *35*(24), L24503. https://doi.org/10.1029/2008gl036127

Nick, F. M., Vieli, A., Howat, I. M., & Joughin, I. (2009). Large-scale changes in Greenland outlet glacier dynamics triggered at the terminus. *Nature Geoscience*, *2*(2), 110–114. https://doi.org/10.1038/ngeo394

Noël, B., van de Berg, W. J., Van Wessem, J. M., Van Meijgaard, E., Van As, D., Lenaerts, J., et al. (2018). Modelling the climate and surface mass balance of polar ice sheets using RACMO2–Part 1: Greenland (1958–2016). *The Cryosphere*, *12*(3), 811–831. https://doi.org/10.5194/tc-12-811-2018

Nye, J. F. (1953). The flow law of ice from measurements in glacier tunnels, laboratory experiments and the Jungfraufirn borehole experiment. *Proceedings of the Royal Society of London. Series A. Mathematical and Physical Sciences*, *219*(1139), 477–489.

Obara, K. (2002). Nonvolcanic deep tremor associated with subduction in southwest Japan. *Science*, *296*(5573), 1679–1681. https://doi.org/10.1126/science.1070378

Park, J., Vernon, F. L., III., & Lindberg, C. R. (1987). Frequency dependent polarization analysis of high-frequency seismograms. *Journal of Geophysical Research*, *92*(B12), 12664–12674. https://doi.org/10.1029/jb092ib12p12664

Podolskiy, E. A., Murai, Y., Kanna, N., & Sugiyama, S. (2021). Ocean-bottom and surface seismometers reveal continuous glacial tremor and slip. *Nature Communications*, *12*(1), 3929. https://doi.org/10.1038/s41467-021-24142-4

Podolskiy, E. A., Sugiyama, S., Funk, M., Walter, F., Genco, R., Tsutaki, S., et al. (2016). Tide-modulated ice flow variations drive seismicity near the calving front of Bowdoin Glacier, Greenland. *Geophysical Research Letters*, *43*(5), 2036–2044. https://doi.org/10.1002/2016gl067743

Podolskiy, E. A., & Walter, F. (2016). Cryoseismology. *Reviews of Geophysics*, *54*(4), 708–758. https://doi.org/10.1002/2016rg000526

Riel, B., Minchew, B., & Joughin, I. (2021). Observing traveling waves in glaciers with remote sensing: New flexible time series methods and application to Sermeq Kujalleq (Jakobshavn Isbræ), Greenland. *The Cryosphere*, *15*(1), 407–429. https://doi.org/10.5194/tc-15-407-2021

Robel, A. A., Tsai, V. C., Minchew, B., & Simons, M. (2017). Tidal modulation of ice shelf buttressing stresses. *Annals of Glaciology*, *58*(74), 12–20. https://doi.org/10.1017/aog.2017.22

Roeoesli, C., Helmstetter, A., Walter, F., & Kissling, E. (2016). Meltwater influences on deep stick-slip icequakes near the base of the Greenland Ice Sheet. *Journal of Geophysical Research: Earth Surface*, *121*(2), 223–240. https://doi.org/10.1002/2015jf003601

Rogers, G., & Dragert, H. (2003). Episodic tremor and slip on the Cascadia subduction zone: The chatter of silent slip. *Science*, *300*(5627), 1942–1943. https://doi.org/10.1126/science.1084783

Schoof, C. (2005). The effect of cavitation on glacier sliding. *Proceedings of the Royal Society A: Mathematical, Physical and Engineering Sciences*, *461*(2055), 609–627. https://doi.org/10.1098/rspa.2004.1350

Schoof, C. (2010). Ice-sheet acceleration driven by melt supply variability. *Nature*, *468*(7325), 803–806. https://doi.org/10.1038/nature09618

Stearns, L. A., & Hamilton, G. S. (2007). Rapid volume loss from two East Greenland outlet glaciers quantified using repeat stereo satellite imagery. *Geophysical Research Letters*, *34*(5), L05503. https://doi.org/10.1029/2006gl028982

Stevens, L. A., Nettles, M., Davis, J. L., Creyts, T. T., Kingslake, J., Ahlstrøm, A. P., & Larsen, T. B. (2022). Helheim Glacier diurnal velocity fluctuations driven by surface melt forcing. *Journal of Glaciology*, *68*(267), 77–89. https://doi.org/10.1017/jog.2021.74

Straneo, F., Curry, R. G., Sutherland, D. A., Hamilton, G. S., Cenedese, C., Våge, K., & Stearns, L. A. (2011). Impact of fjord dynamics and glacial runoff on the circulation near Helheim Glacier. *Nature Geoscience*, *4*(5), 322–327. https://doi.org/10.1038/ngeo1109

Tsai, V. C., Smith, L. C., Gardner, A. S., & Seroussi, H. (2022). A unified model for transient subglacial water pressure and basal sliding. *Journal of Glaciology*, *68*(268), 390–400. https://doi.org/10.1017/jog.2021.103

Tsai, V. C., Stewart, A. L., & Thompson, A. F. (2015). Marine ice-sheet profiles and stability under Coulomb basal conditions. *Journal of Glaciology*, *61*(226), 205–215. https://doi.org/10.3189/2015jog14j221

Tulaczyk, S., Kamb, W. B., & Engelhardt, H. F. (2000). Basal mechanics of ice stream B, west Antarctica: 1. Till mechanics. *Journal of Geophysical Research*, *105*(B1), 463–481. https://doi.org/10.1029/1999jb900329

Ultee, L. (2021). ehultee/helheim-fiesta: Initial pre-release (v0.1-alpha) [Dataset]. Zenodo. https://doi.org/10.5281/zenodo.4707997

Ultee, L., Felikson, D., Minchew, B., Stearns, L. A., & Riel, B. (2022). Helheim Glacier ice velocity variability responds to runoff and terminus position change at different timescales. *Nature Communications*, *13*(1), 6022. https://doi.org/10.1038/s41467-022-33292-y

Umlauft, J., Lindner, F., Roux, P., Mikesell, T. D., Haney, M. M., Korn, M., & Walter, F. T. (2021). Stick-slip tremor beneath an alpine glacier. *Geophysical Research Letters*, *48*(2), e2020GL090528. https://doi.org/10.1029/2020gl090528

Van den Broeke, M. R., Enderlin, E. M., Howat, I. M., Kuipers Munneke, P., Noël, B. P., Van De Berg, W. J., et al. (2016). On the recent contribution of the Greenland ice sheet to sea level change. *The Cryosphere*, *10*(5), 1933–1946. https://doi.org/10.5194/tc-10-1933-2016

Vaňková, I., Voytenko, D., Nicholls, K. W., Xie, S., Parizek, B. R., & Holland, D. M. (2018). Vertical structure of diurnal englacial hydrology cycle at Helheim Glacier, East Greenland. *Geophysical Research Letters*, *45*(16), 8352–8362. https://doi.org/10.1029/2018gl077869

VanWormer, D., & Berg, E. (1973). Seismic evidence for glacier motion. *Journal of Glaciology*, *12*(65), 259–265. https://doi.org/10.3189/s002214300003207x

Vore, M. E., Bartholomaus, T. C., Winberry, J. P., Walter, J. I., & Amundson, J. M. (2019). Seismic tremor reveals spatial organization and temporal changes of subglacial water system. *Journal of Geophysical Research: Earth Surface*, *124*(2), 427–446. https://doi.org/10.1029/2018jf004819

Voytenko, D., Stern, A., Holland, D. M., Dixon, T. H., Christianson, K., & Walker, R. T. (2015). Tidally driven ice speed variation at Helheim Glacier, Greenland, observed with terrestrial radar interferometry. *Journal of Glaciology*, *61*(226), 301–308. https://doi.org/10.3189/2015jog14j173

Walter, F., Deichmann, N., & Funk, M. (2008). Basal icequakes during changing subglacial water pressures beneath Gornergletscher, Switzerland. *Journal of Glaciology*, *54*(186), 511–521. https://doi.org/10.3189/002214308785837110

Wang, X., Voytenko, D., & Holland, D. M. (2022). Accuracy evaluation of digital elevation models derived from terrestrial radar interferometer over Helheim Glacier, Greenland. *Remote Sensing of Environment*, *268*, 112759. https://doi.org/10.1016/j.rse.2021.112759

Weaver, C. S., & Malone, S. D. (1979). Seismic evidence for discrete glacier motion at the rock–ice interface. *Journal of Glaciology*, *23*(89), 171–184. https://doi.org/10.3189/s0022143000029816

Weertman, J. (1957). On the sliding of glaciers. *Journal of Glaciology*, *3*(21), 33–38. https://doi.org/10.3189/s0022143000024709

Wessel, P., Luis, J. F., Uieda, L., Scharroo, R., Wobbe, F., Smith, W. H., & Tian, D. (2019). The generic mapping tools version 6.[Software]. Geochemistry, Geophysics, Geosystems, *20*, 5556–5564. https://doi.org/10.1029/2019GC008515

Wiemer, S., & Wyss, M. (2002). Mapping spatial variability of the frequency-magnitude distribution of earthquakes. In *Advances in geophysics* (Vol. 45, p. 259). Elsevier.

Winberry, J. P., Anandakrishnan, S., Wiens, D. A., & Alley, R. B. (2013). Nucleation and seismic tremor associated with the glacial earthquakes of Whillans Ice Stream, Antarctica. *Geophysical Research Letters*, *40*(2), 312–315. https://doi.org/10.1002/grl.50130

Xie, S., Dixon, T. H., Holland, D. M., Voytenko, D., & Vaňková, I. (2019). Rapid iceberg calving following removal of tightly packed pro-glacial mélange. *Nature Communications*, *10*(1), 3250. https://doi.org/10.1038/s41467-019-10908-4

Yan, P., Holland, M. D., Tsai, C. V., Vaňková, I., & Xie, S. (2023a). Line of Sight (LOS) velocity obtained from terrestrial radar interferometer at Helheim Glacier [Dataset]. Zenodo. https://doi.org/10.5281/zenodo.8172884

Yan, P., Holland, M. D., Tsai, C. V., Vaňková, I., & Xie, S. (2023b). Processed ApRES displacement of internal reflectors at Helheim Glacier in August, 2016 [Dataset]. Zenodo. https://doi.org/10.5281/zenodo.8161341

Yan, P., Holland, M. D., Tsai, C. V., Vaňková, I., & Xie, S. (2023c). Seismic waveform data collected at Helheim Glacier between Aug, 2012 and Jun, 2017 (part 1) [Dataset]. Zenodo. https://doi.org/10.5281/zenodo.8173507

Yan, P., Holland, M. D., Tsai, C. V., Vaňková, I., & Xie, S. (2023d). Seismic waveform data collected at Helheim Glacier between Aug, 2012 and Jun, 2017 (part 2) [Dataset]. Zenodo. https://doi.org/10.5281/zenodo.8174155

Zoet, L. K., Anandakrishnan, S., Alley, R. B., Nyblade, A. A., & Wiens, D. A. (2012). Motion of an Antarctic glacier by repeated tidally modulated earthquakes. *Nature Geoscience*, *5*(9), 623–626. https://doi.org/10.1038/ngeo1555

Zoet, L. K., & Iverson, N. R. (2020). A slip law for glaciers on deformable beds. *Science*, *368*(6486), 76–78. https://doi.org/10.1126/science.aaz1183

## References From the Supporting Information

Barruol, G., Cordier, E., Bascou, J., Fontaine, F. R., Legrésy, B., & Lescarmontier, L. (2013). Tide-induced microseismicity in the Mertz glacier grounding area, East Antarctica. *Geophysical Research Letters*, *40*(20), 5412–5416. https://doi.org/10.1002/2013gl057814

Tsai, V. C., Minchew, B., Lamb, M. P., & Ampuero, J. P. (2012). A physical model for seismic noise generation from sediment transport in rivers. *Geophysical Research Letters*, *39*(2), L02404. https://doi.org/10.1029/2011gl050255